Electronic Supplementary Material (ESI) for Lab on a Chip.

Supplemental Information

Application of a Gut-Liver-on-a-Chip Device and Mechanistic Modelling to the Quantitative In Vitro Pharmacokinetic Study of Mycophenolate Mofetil

Nicoló Milani[1,2], Neil Parrott[1], Daniela Ortiz Franyuti[1], Patricio Godoy[1], Aleksandra Galetin[2], Michael Gertz[1], and Stephen Fowler[1]

[1] Pharmaceutical Sciences, Roche Pharma Research and Early Development, Roche Innovation Center Basel, Grenzacherstrasse 124, 4070, Basel, Switzerland.

[2] Centre for Applied Pharmacokinetic Research, University of Manchester, UK

Contents

Contents of tables and figures

TABLES

FIGURES

1. Pre-incubation protocol

1.1 Caco2 and HT29 Coculture Medium Exchange

- 24 transwells with already seeded Caco2 and HT29 cells (seeding density ranging between 150,000 and 180,000 cells/well) were delivered by ReadyCells at Day -5 or Day -4 (Figure 2). From the day of the plate delivery to day -3 the cells are maintained at room temperature in the delivery package in the transportation gel which needs to be replaced at Day -3 with the differentiation medium.
- The plate was placed in the incubator for 4 hours in order to liquefy the delivery medium. Then the delivery medium was aspirated in the basolateral and apical side. This procedure has to be done very carefully. 700 µL of pre-warmed differentiation medium (37 ºC) was added to the plate in the basolateral side and 300 µL in the apical side.
- The plate was returned to the incubator until Day 0.

1.2 Plate preparation

- At Day -5 (Figure 3), the TL-6 plates and the PhysioMimixTM MPS Drivers were first wiped with 70% ethanol and afterwards combined. The TL-6 plate was primed using 400 µL of the pre-warmed plating medium at 37 ºC in the liver compartment (opposite direction of the scaffold) the day before seeding the hepatocytes. The drivers with the attached TL-6 plates were placed in the incubator and connected with the docking station.

1.3 Plate priming.

- The specific program “Prime” was performed and it induced a flow of 150 µL/min for 3 minutes (Figure 3).
- After this program, the plate was removed from the incubator and additional 1100 µL of plating medium was added to the liver chamber in order to completely cover the surface of the well.
- The plate was returned to the docking station inside the incubator and the “Incubation” program run, which induces an upwards flow of 60 µL/s until the seeding day (Day -4).

1.4 Hepatocyte seeding.

- At Day -4 (Figure 3) the plates were removed from the incubator and the old medium was aspirated away with exception of 200 µL of dead volume.
- 400 µL of fresh plating medium was added and the “Media Exchange" program was performed for 3 minutes at a flow rate of60µL/min.
- After 3 minutes, the medium was aspirated away (200 µL dead volume remaining) and it was ready for the seeding process.
- In order to perform the seeding, the cryopreserved hepatocyte recovery medium (CHRM) and plating medium were pre-warmed to 37 °C in the water bath. Hepatocyte vial(s) were thawed, and

the cells were transferred and suspended in 50 mL of CHRM. The cell suspension was centrifuged at room temperature at 100G for 10 minutes, and afterwards, the supernatant was carefully removed. Hepatocyte pellet was loosened by gently tapping the falcon tube and re-suspended in 3.0 mL (for two vials of hepatocytes) of plating medium. 50 µL of cell suspension was transferred to 0.1% Trypan Blue for the cell count with the hemocytometer.

- 300 µL plating medium was added to plates having 200 µL of dead volume in order to prepare the plates for the seeding process and then the suspension of hepatocytes was carefully distributed to each scaffold (100 µL for each well) for gut-liver and liver only assessment.
- The plates were returned to the docking station to run the "Seed" program, which induces a downwards flow of 60 µL/min for 2 minutes.
- The plates were removed and 1000 µL of plating medium was very slowly added to the wells to cover the surface of the wells.
- The plates were returned to the docking station and the "Seed" program run for an additional 8 hours after which the "Incubate" program was run with upwards flow of 60 µL/min. For the wells used for gut-only assessment all the procedures described above were followed but using a plating medium without suspended hepatocytes.

1.5 Media exchange.

- At day -3, the plating medium was replaced with fresh maintenance medium (Figure 3). To do that, the TL-6 plate was removed from the docking station and the medium was aspirated away (leaving 200 µL of dead volume).
- 400 µL of pre-warmed (at 37 °C) maintenance medium was added to the plate which was returned to the incubator. The "Medium Exchange" was performed for 3 minutes and then the plates were detached from the docking station and the medium was aspirated away.
- 1400 µL of medium was added in order to cover the well surface and the plate was returned again in the incubator. The "Incubate" program was performed until the start of the experiment at Day 0.

2. Incubation protocol

- At day 0 (Figure 2), 24 Caco2-HT29 cells transwell cultures (pretreated for a week before the experiment) were removed from the incubator and barrier integrity assessed by transepithelial electrical resistance (TEER) measurement.
- The best six transwells having the highest electrical resistance were selected to be used in the experiment. The TL-6 plate was removed from the incubator and the maintenance medium was aspirated away from the liver chamber (residual volume 200 µL).
- 400 µL of medium was added to the liver chamber and the "Medium Exchange" program was run for 3 minutes. Then, the medium was aspirated away and 1950 µL of maintenance medium was added (in total 2150 µL considering the dead volume of 200 µL).
- An additional priming step with the interconnection flow between the gut basolateral side and the liver was performed for gut-liver and gut-only system. The liver compartment flow rate during the priming was set at 60 µL/min for liver-only system (no basolateral and interconnection flow was used). The interconnection flow, the basolateral flow and the liver compartment flow were set at 150, 30, and 60 µL/min, respectively as the manufacturer recommended in the gut-liver and gut-only systems. The flow regimes were maintained for 4.5 hours before the start of the experiment.
- In the meantime, the transwells were rinsed with apical maintenance medium and a pre-warmed (37 ºC) solution of apical maintenance medium was added (325 µL to the apical side and 750 µL to the basolateral side). This procedure was repeated another 2 times.
- At the end of this additional priming step, the TL-6 plate was moved from the incubator to the laminar flow cabinet and 325 µL of intestinal maintenance medium containing 10 µM of the test compound was added in the apical side of the transwell in the gut-liver and gut-only systems. In the liver only system the test compound (1 µM) was added directly to the liver chamber in the hepatocyte maintenance media.

- The initial time point was sampled directly after the addition of the medium. After, the plate was put again in the docking station and all the programs in the liver chamber, basolateral, and interconnection were activated again. The liver compartment flow rate during the incubation was set at 150 µL/min in the liver-only system. The interconnection flow, the basolateral flow and the liver chamber flow were set at 90, 60, and 90 µL/s, respectively for gut-liver and gut-only systems. All the flow rates in the gut and liver compartments were selected in order to maintain a mix stirred condition in the respective compartment.

At each sampling point the TL-6 plate was moved to the cabinet switching off all the flows in each compartment (static system) for as short a time as possible (2 min). Afterwards, the flows were re-established as reported above.

3. Chromatography and MS/MS parameters

Mycophenolate Mofetil and its metabolites	
Total flow (mL/min)	0.900
Column	Supelco Ascentis® Express 90 Å AQ-C18, 2.7 µm HPLC Column L × I.D. 2 cm × 3 mm
Column Temp. (°C)	50
Injection volume	8 µL in 2 µL loop
Solvent A	Water + 0.1% HCOOH
Solvent B	AcN + 0.1% HCOOH
Time (min)	**% Solvent B**
0	5
0.85	98
1.00	98
1.01	5
1.20	5

Table S3.1. Chromatography program

Compound	Q1 (Da)	Q2 (Da)	DP (volts)	EP (volts)	CE (volts)	CXP (volts)	RT (min)
Mycophenolate Mofetil	434.300	114.100	80.000	10.000	38.000	8.000	0.40
MPA	319.00	275.000	-80.000	-10.000	-28.000	-32.000	0.50
MPAG	495.000	319.000	-80.000	-10.000	-28.000	-32.000	0.35

Table S3.2. Basic MS/MS parameters in MRM acquisition mode and RT

4. TEER measurements

The TEER measurements (Transepithelial Electrical Resistance) were performed to assess the health of the cellular monolayers before starting the experiment and at the end of the incubation. A EVOM2 (World Precision Instrument) with STX100 series of electrodes was used to assess the monolayer quality of Caco2-HT29 cells. The electrode was immersed in a 70% solution of EtOH in water to be sterilized. Then, it was immersed in a solution of medium for a few seconds in order to remove the eventual presence of EtOH solution in the electrode. Before the analysis the transwells in a 24 wells plates was conditioned for 30 minutes at room temperature. The electrical resistance was multiplied by the area of the transwell (0.33 cm^2) and compared to the minimum value recommended by ReadyCells. (70 Ω cm^2):

$$TEER\ (\Omega \cdot\ cm^2) = R_{cells}\ (\Omega)\ \cdot Area\ (cm^2)$$ (equation S1)

5. Caco2 and HT29 cells monolayer by CLSM

In addition to TEER measurements as means to assess the integrity of the cellular monolayers, confocal light scanning microscopy images were acquired after the experiments were finalized to evaluate the integrity and coverage of the Caco2 and HT29 cells monolayer. The apical and the basolateral media were aspirated and the transwells placed in a 24-well plate with a solution of 4% of paraformaldehyde in PBS added to both apical and basolateral sides to fix the cells. The solution was left for 20 minutes to complete the treatment. Afterwards the solution was aspirated from both apical and basolateral sides and a solution of PBS was added to wash away the fixing solution. This washing process was repeated twice and the transwells were stored at 4 ºC until the confocal laser scanning microscopy (CLSM) measurements. The cells were stained for nuclei and actin network using a solution of 1% of Triton X, DAPI (1:1000) and A647-Phalloidin (1:200) after removing the PBS solution in the apical and basolateral side. The plate with the transwells was left for 20 minutes covered with aluminum foil. Afterwards, the solution was aspirated from both sides and the transwells were washed 3 times with PBS. In order to assess using CLSM, each transwell was very carefully detached from the insert with a scalpel and placed on a glass slide. . From the image stacks, nuclei were detected using the in-built 3D surface segmentation algorithms found in the software Imaris 6.3 (Bitplan, Zurich, Switzerland). The same algorithm was used to select the area covered by an actin network, and thereby confirm the integrity of the monolayer. See Figure S1. From the images, homogeneous nuclei coverage and distribution, as well as a homogeneous actin network spanning the monolayer confirmed an intact monolayer of cells present on the samples.

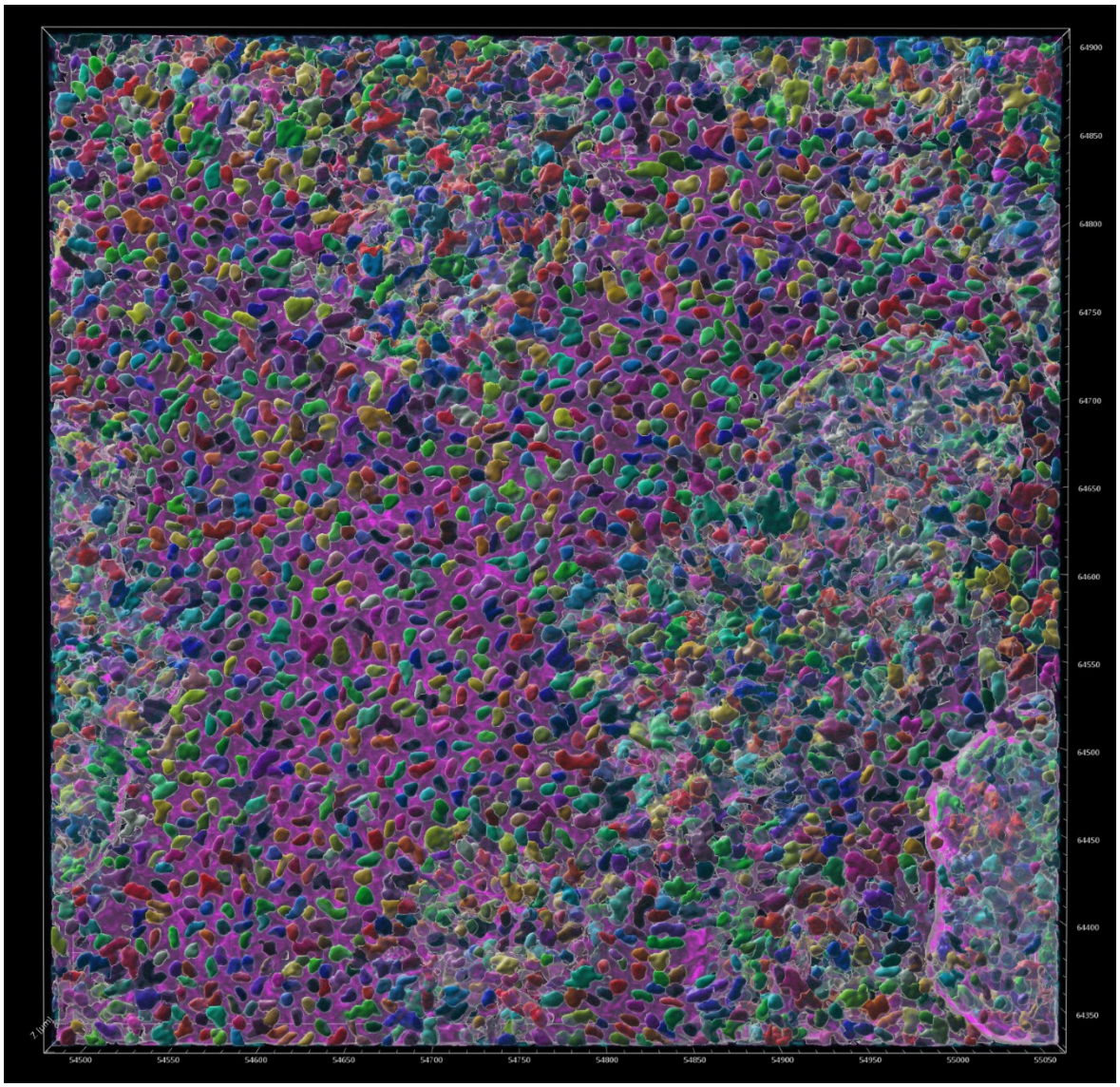

Figure S5.1. Caco2 and HT29 cells monolayer after 24 h of incubation detected by CLSM. Homogeneous nuclei coverage and distribution (Nuclei stained with DAPI, segmented and coloured randomly to assess the monolayer coverage), as well as a homogeneous actin network (A647-Phalloidin stain, 3D-Area segmented to assess coverage) confirmed an intact monolayer of cells present on the samples after concluding the experiments. Images acquired with a Leica SP8 Confocal Microscope fitted with an HC PL APO CS2 oil immersion 20x objective. Image analysis performed using Imaris 6.3, Surface 3D registration/segmentation algorithms.

6. Model generation and verification of assumptions

Introduction

Robust estimation of in vitro parameters is essential for correct prediction of in vivo PK. In the specific case of the Gut-Liver OoC and using MM as test compound, the complexity of the system and the PK requires a careful evaluation of the in silico models capable of describing the experimental data. As a consequence, this sections reports evaluations that have led to the generation of the model used for fitting in the gut-liver systems. Preliminary fitting for the gut-liver system was performed in order to capture the most important PK processes in the system and they were mostly based on a pilot experiment and the data from the gut-only and liver-only systems. First, a *General Model* was proposed which was close to the actual experimental conditions. The *General Model* considered the assumption of a rapid equilibrium of MPA and MPAG between the hepatocytes and the media. It was found that some processes of *General Model* could be simplified, and *Model 1* was proposed. Afterwards, *Model 1* was simplified in order to further reduce unnecessary complexity by comparing it with *Model 2* and *3*.A schematic representation and the results verification of the models is provided in Table S3 and a more detailed explanation is reported in the next paragraphs. Additional evaluation such as the impact of the intestinal cells volume (Figure S10 and Table S7) and the Q_i (interconnection media flow rate) (Table S8) uncertainty were performed for *Model 1*. The model validity reported in this work were demonstrated and verified using simulations in accordance with the most likely experimental conditions and compound-related PK parameters or by a fitting approach and they are explained in detail in the next paragraphs.

In conclusion, all the DMPK parameters in the main manuscript were generated from *Model 1* and all the details are reported in the next paragraphs. However, it is important to remark that for each device, experimental system, and test compound a specific model need to be generated and verify as we reported in this work.

Table S6.1. Summary of the main feature of the General Model, Model 1, 2, and 3.

*Sampling in the liver compartment included also that in the basolateral side. A more detailed description of the models is described in the newt paragraphs. Degree of complexity is reduced from +++ to +

		Volume			Q_i	Verification
Complexity	**Model**	**Apical side**	**Basolateral side**	**Liver**		
+++	*General model*	Sampling	Sampling	- Sampling - Evaporation	Interruption for sampling	Unnecessary
++	*Model 1*	Sampling	Constant	- Sampling* - Evaporation	No interruption	Accepted
+	*Model 2*	Constant	Constant	- Sampling* - Evaporation	No interruption	Rejected
+	*Model 3*	Sampling	Constant	Constant	No interruption	Rejected

6.1 General Model

The introduction in the model of additional complexity to the DMPK processes was supported by experimental observations which are described below. The sampling volume in the apical side was 25 µL which represents > 25% of the initial volume of media in this compartment (Figure S2-A). Therefore it was especially important for the model to consider the media depletion and the removal of the amount of drug and metabolites from the sampling volume at the specific time points in the gut-apical side (Figure S2-B). In addition, media evaporation (experimentally evaluated) and the sampling volume in the basolateral and liver compartments were included in order to represent the actual experimental system. The media evaporation depends on the surface of the compartments and it was considered for the basolateral side and liver compartment. The apical side was not considered to have a large impact in the media evaporation. The experimental k_{ev} (0 order constant), considered the contribution of both basolateral and liver compartments:

$$k_{ev,i}(Liver) = \frac{A_L}{A_L + A_B} k_{ev,i} \qquad \text{(equationS2)}$$

$$k_{ev,i}(Basol.) = \frac{A_B}{A_L + A_B} k_{ev,i} \qquad \text{(equationS3)}$$

Where A_L and A_B are the surface area of the liver and basolateral compartment, respectively; and $k_{ev,i}$(Liver) and $k_{ev,i}$(Basol.) the media evaporation rate in the liver and basolateral compartment for the well i. However, it was demonstrated that the evaporation and the sampling volume can be considered to happen only in the liver compartment since the fast re-fill of media from the liver compartment to the basolateral side to maintain the maximum volume of 1506 µL (Figure S2-A and B) (see *General Model* evaluation). Therefore in the equation above A_B was considered equal to 0 and $k_{ev,i}$(Liver)=$k_{ev,i.}$

In addition, to the described features, the general model took into account that the Q_i is interrupted at any sampling time since the plate is not attached to the dock-station. Indeed, the flow system regimen between the basolateral and the liver chamber maintained the media volume in the basolateral side constant overtime. Indeed, the media flowed from the liver chamber to the basolateral side thanks to the micropumps activation, but it spilled over from the basolateral to the liver chamber by gravity after reaching the highest level of the basolateral side volume. The delay of the actual re-start of the flow rate allowed a small extent of compound accumulation in the respective compartment in which they were located when the media flow was interrupted. In particular, this effect might be influential in the initial sampling times and in particular when equilibration between basolateral and liver compartments was not yet reached. The time necessary to return to the maximum volume (1506 µL) in the basolateral side with a Q_i of 90 µL/min after a sampling volume of 25 µL was 17 seconds, which was small in relation to the total length of incubation and less than the time taken for plate removal from the docking station during the sampling process. The time necessary for the

actual sampling is hard to generalize because it depends on the number of the compartments involved in the sampling. That process was performed as fast as possible and was less than 2 minutes per plate.

A

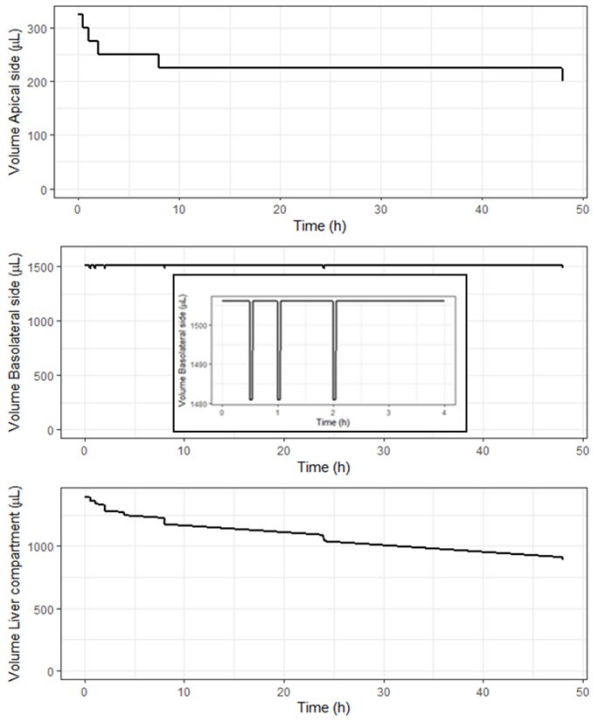

B

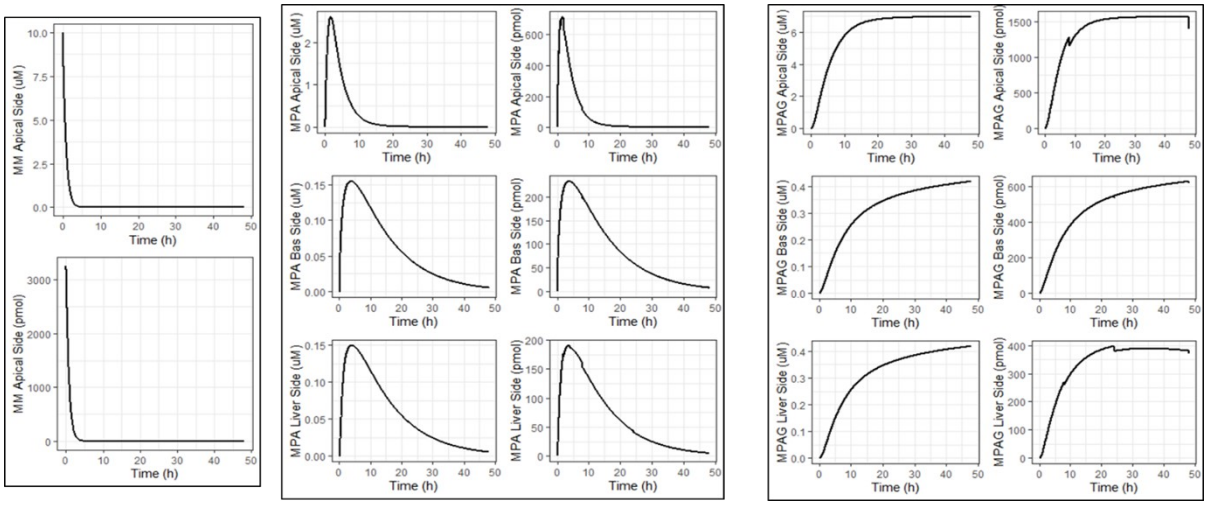

Figure S6.1. Simulation from *General Model*. A) Graphical representation of the media volume in all compartments, B) compound concentration and amount over the incubation time in all sampled compartments. Simulation was performed using the input data in Table S3 and without inter-well variability of Q_i, number of hepatocytes and intestinal cells, and k_{ev}.

6.2 Model 1

Model 1 was a simplification of the *General Model* and the difference was the assumption of a constant Q_i (no interruption for sampling) and that the sampling volume in the basolateral compartment happened in the liver compartment (Figure S3). Therefore the aim of this investigation was to prove from simulations if the additional complexity of the *General Model* impacted or not the PK estimation. In case the simulations from both model provided negligible differences, the additional complexity in the General Model is not necessary and it avoids the development of complicate fitting model. The data from the simultaneous fitting (Table S4) were used as input data in simulations of both *Model 1* and *General Model*.

A

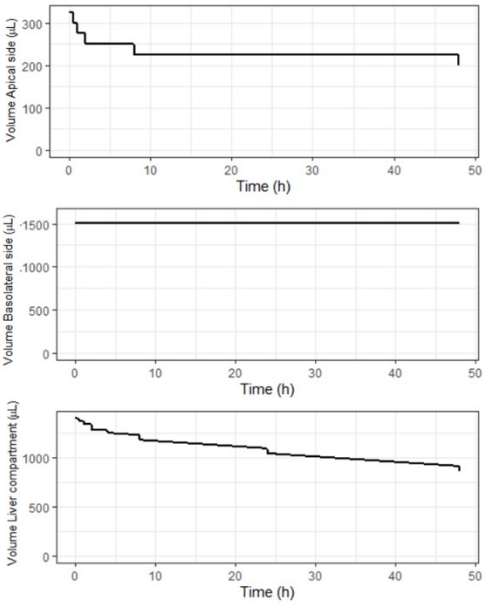

B

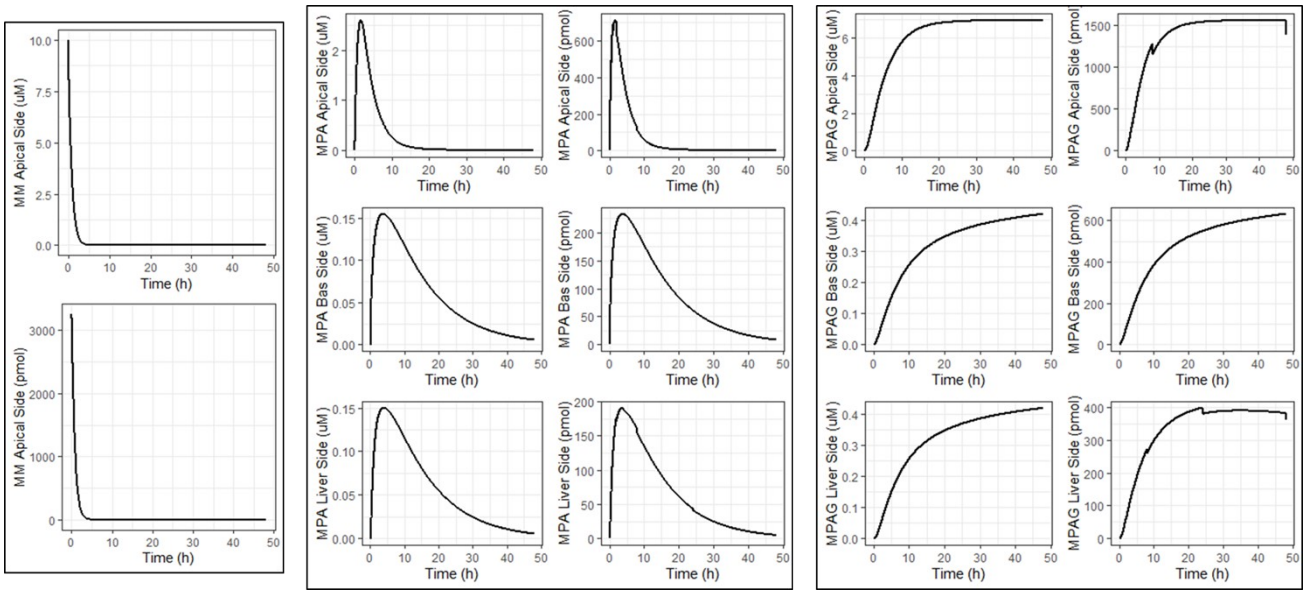

Figure S6.2. Simulations from *Model 1*. A) Graphical representation of the media volume in all compartments, B) compound concentration and amount over the incubation time in all sampled compartments. Simulation was performed using the input data in Table S4 and without inter-well variability of Q_i, number of hepatocytes and intestinal cells, and k_{ev}.

Parameter feature	Parameter	Units	Value
PK parameter from simultaneous estimation	$CL_{int,gut,u}$ (MM)	µL/min/10^6 cells	13
	$CL_{int,gut,u}$ (MPA)	µL/min/10^6 cells	17
	$CL_{app,hep,u}$ (MPA)	µL/min/10^6 cells	26
	P_{app} (MPA)	nm/s	546
	P_{app} (GMPA)	nm/s	0.32
	E_r (MPA)		3.0
	E_r (MPAG)		3.1
PK parameter experimentally estimated	fu_{inc} apical (all compounds)		1
	fu_{inc} bas (MPA)		0.38
	fu_{inc} bas (MPAG)		0.70
System	Initial V_{apical}	µL	325
	Initial $V_{basolateral}$	µL	1506
	Initial $V_{liver\ comp.}$	µL	1394
	Surface transwell	cm^2	0.33
	Volume of gut cells V_e	µL/10^6	2.6
Experimentally observed	Initial conc. in the apical side	µM	10
	Interconnection flow (Q_i)	µL/min	90 (20%)
	Number intestinal cells	10^6 cells	0.45 (15%)
	Number hepatocytes	10^6 cells	0.30 (15%)
	Sample volume	µL	25
	k_{ev}	µL/min	0.09 (15%)

Table S6.2. Parameters used in the simulations reported for the modelling verification. The number in the brackets represents the respective uncertain as CV%. The uncertainty was determined from experimental observation for the number of hepatocyte, intestinal cells and k_{ev} and was settled 15% also if those observed were 10, 11, and 14%, respectively. The uncertainty of Q_i was provided by CN Bio Ltd.

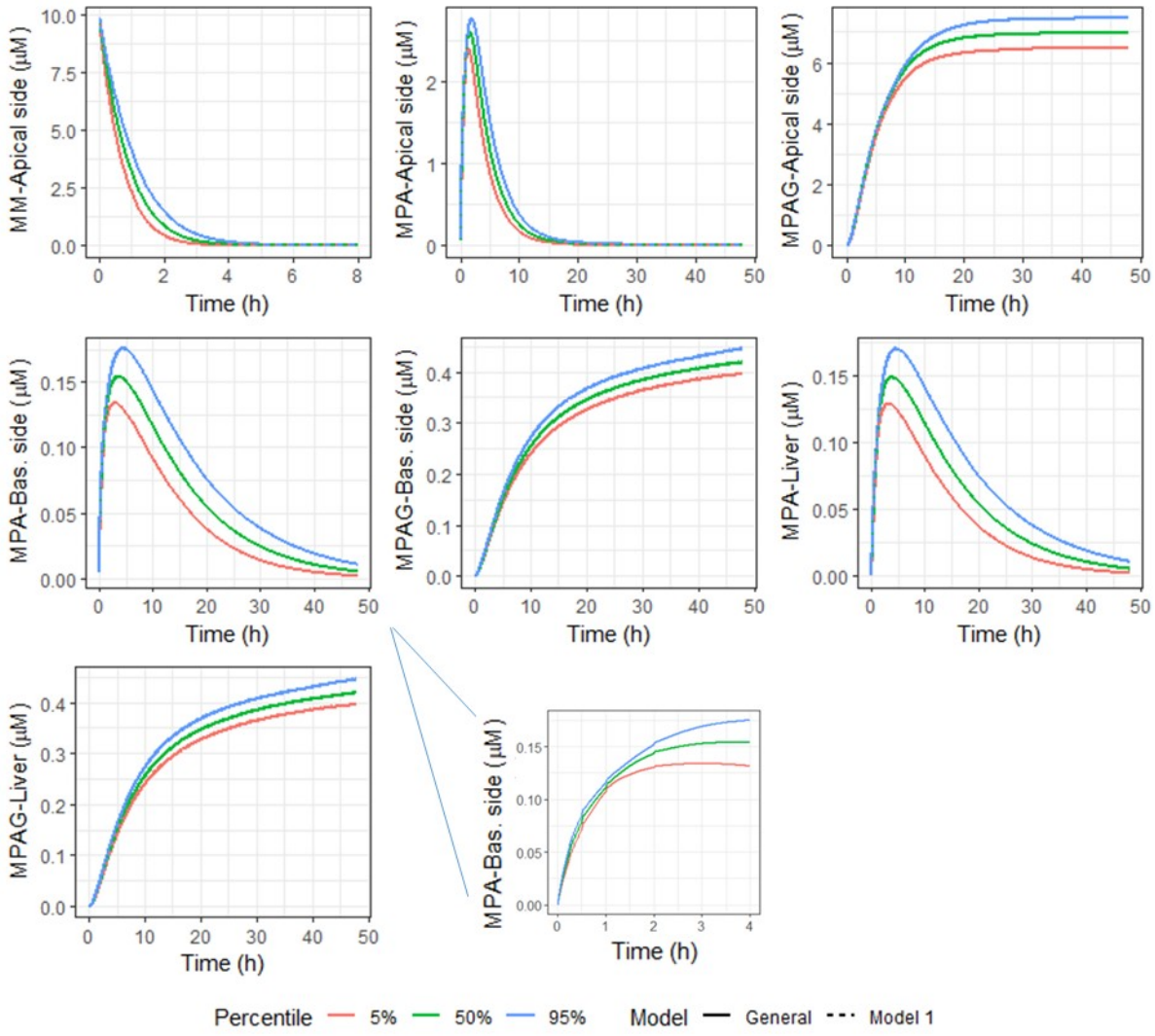

Figure S6.3. 1000 simulations from the *General* and *Model 1* with a percentile of 5-50-95% from the coefficient of variation associated with the k_{ev}, number of gut and liver cells of 15% and Q_i with a CV of 20 and respectively (Table S4). Simulation of MPA in the basolateral side in a time window of 4 h. Accumulation of compounds was observed from the general model when Qi is 0 during the sampling. However, the effect of the compound accumulation in the compartment is negligible. As an example it is possible to see in the time-concentration profile (General Model) of MPA in the basolateral side very little divergences between 0 and 2 h which are the consequence of the 2 minute of Q_i interruption for sampling. However, due to the overlap of the two simulations, the divergences in the MPA profiles were hardly detectable it was reported in a dedicated Figure S4. However, it was clear that the blocking of Q_i and the delay to re-establish the constant volume in the basolateral side were negligible.

The simulations in Figure S4 showed a clear overlap of the time-concentration-profiles which did not allow to observe any appreciable difference from the two models for all compounds and in every compartment. Therefore, it was proved that the difference in the PK profiles of all compounds in all compartments between

the *General Model* and *Model 1* was abundantly below the accuracy (> 90%) of the analytical method. The *General Model* was unnecessary since it did not bring significant difference in this condition of DMPK processes, Q_i, and interval of sampling and it made possible to avoid to implement a complex fitting model. However, as reported in this work, a rigorous verification should be perform for each experimental system and test compound. In general, in order to avoid significant impact on the estimates, we suggested to reduce the interval for sampling as much as possible and diminish the time of Q_i interruption.

6.3 Model 2

Model 1 was applied in comparison with the approximated *Model 2* which did not consider the media sampling in the apical side. As expected a significant decrease of the concentration in the apical side of MPAG was detected in *Model 1* compared to *Model 2* (Figure S5). On the other hand, a reduction of the highest concentration of MPA and MPAG was also highlighted in the basolateral and liver compartment.

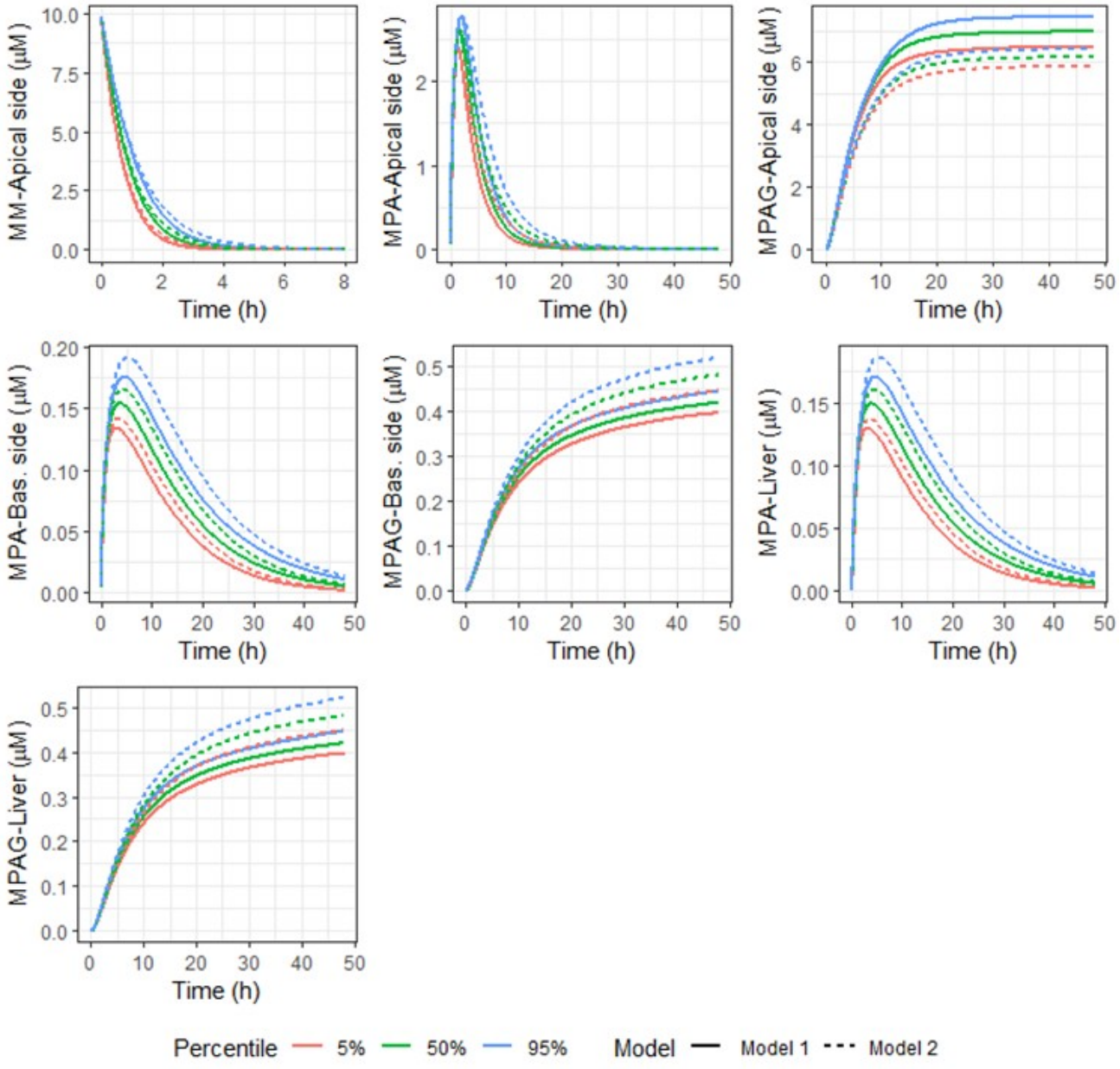

Figure S6.4. 1000 simulations from *Model 1* and *Model 2* with a percentile of 5-50-95% using the input data from Table S3.

Additional information on the effect of evaporation were also provided by fitting the gut-liver, gut-only, and simultaneous (gut-liver, gut-only, and liver-only) fitting data without sampling in the apical side (1) and

considering the sampling in that compartment (2) (Table S5). All parameters of MPA were influenced by the sampling in the apical side and in particular $CL_{int,gut,u}$ (MPA). In gut-only and simultaneous fitting (all) conditions for which the parametric uncertainty was less, the impact of the sampling for MPA PK parameters was better highlighted than in the gut-liver system. From the simulations and fitting was clear that the simplification proposed was not acceptable and therefore it was rejected.

Parameter	**Units**	**Model 1**	**Model 2**	**Model 1**	**Model 2**	**Model 1**	**Model 2**
		Gut-Liver		Gut-Only		Simultaneous	
$CL_{int,gut,u}$(MM)	µL/min/10^6 cells	13 ±1	14 ± 2	12 ± 1	13 ± 1	13 ± 1	14 ± 1
$CL_{int,gut,u}$ (MPA)	µL/min/10^6 cells	24 (13,48)	36 (19,70)	14 ± 1	19 ± 1	17 ± 2	22 ± 2
$CL_{app,hep,u}$ (MPA)	µL/min/10^6 cells	26 (18,30)	24 (14,30)			26 ± 1	25 ± 1
P_{app} (MPA)	nm/s	688 (380,1390)	914 (481,1798)	539 ± 96	655 ± 124	546 ± 73	636 ± 79
P_{app} (MPAG)	nm/s	0.37 ± 0.07	0.33± 0.07	0.39 ± 0.07	0.37 ± 0.07	0.35 ± 0.05	0.32 ± 0.05
E_r (MPA)		3.7 (2.7,5.6)	4.8 (3.4,7.4)	2.7 ± 0.5	3.2 ± 0.7	3.0 (2.7,3.5)	3.6 (3.3,4.0)
E_r (MPAG)		2.9 ± 0.6	3.2 ± 0.7	3.1 ± 0.6	3.6 ± 0.8	3.1 ± 0.5	3.5± 0.6
$CL_{app,hep,u}$ (MM)						639 (565,1054)	639 (565,1054)

Table S6.3. The data using *Model 1* and *Model 2* for fitting reported a significant difference in the parametric estimation of $CL_{int,gut,u}$ (MPA), P_{app} (MPA) and E_r (MPA) in gut-liver system. In brackets range of parameter with confidence level (CL) of 95% from log likelihood profiling when non-normal distribution was observed.

6.4 Model 3

In order to assess the effect of the evaporation and sampling volume in the two different simulations the simplified *Model 3* was applied in comparison with the simplified *Model 1*. *Model 3* had the same characteristics of the *Model 1* except that it did not include the sampling in the basolateral side and in the liver compartment. In addition, it did not include the depletion of media by evaporation. Figure S6 reported the different profiles and their quite significant difference in the basolateral and liver compartment for MPAG.

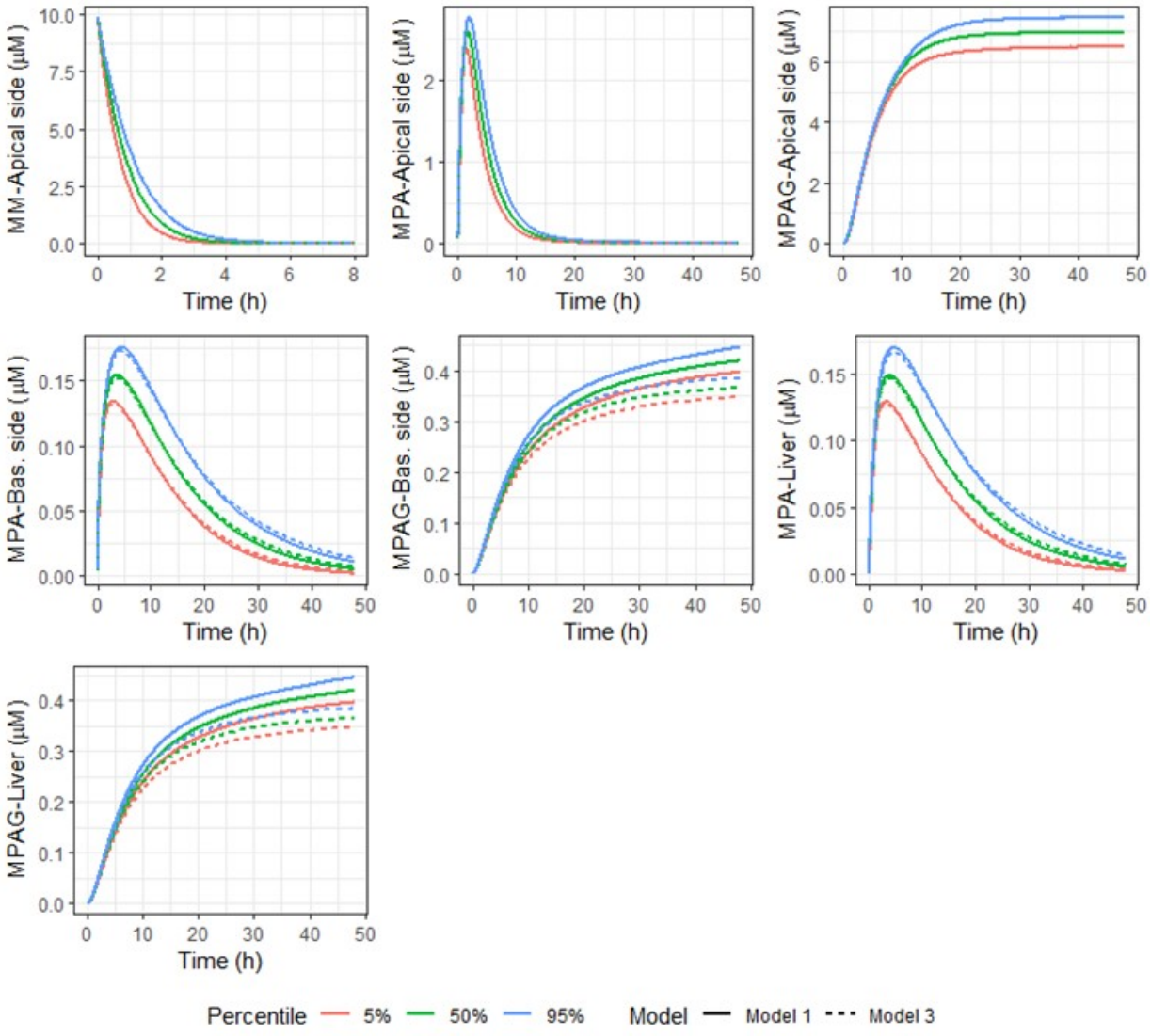

Figure S6.5. 1000 simulations from *Model 1* and *Model 3* with the percentile of 5-50-95% using the input data from Table S3.

Additional analysis to compare both models was executed by fitting as reported in Table S6.

		Condition basolateral + liver sampling & media evaporation					
Parameter	Units	Model 1	Model 3	Model 1	Model 3	Model 1	Model 3
		Gut-Liver		Gut-Only		Simultaneous	
$CL_{int,gut,u}$ (MM)	µL/min/10^6 cells	13 ±1	12 ± 1	12 ± 1	12 ± 1	13 ± 1	13 ± 1
$CL_{int,gut,u}$ (MPA)	µL/min/10^6 cells	24 (13,48)	21 (12,43)	14 ± 1	14 ± 1	17 ± 2	16 ± 2
$CL_{app,hep,u}$ (MPA)	µL/min/10^6 cells	26 (18,30)	30 (22,35)			26 ± 1	29 ± 1
P_{app} (MPA)	nm/s	688 (380,1390)	675 (380,1352)	539 ± 96	535±96	546 ± 73	547 ± 77
P_{app} (MPAG)	nm/s	0.37 ± 0.07	0.38 ± 0.07	0.39 ± 0.07	0.42± 0.07	0.35 ± 0.05	0.37 ± 0.05
E_r (MPA)		3.7 (2.7,5.6)	3.5 ± (2.6,5.2)	2.7 ± 0.5	2.6 ± 0.5	3.0 (2.7,3.5)	2.9 (2.6,3.4)
E_r (MPAG)		2.9 ± 0.6	2.8 ± 0.5	3.1 ± 0.6	2.8 ± 0.5	3.1 ± 0.5	2.8 ± 0.4
$CL_{app,hep,u}$ (MM)						639 (565,1054)	640 (565,1054)

Table S6.4. The data using *Model 1* and *Model 3* for fitting reported a quite significant difference in the parametric estimation of $CL_{app,hep}$ (MPA). In brackets range of parameter with confidence level (CL) of 95% from log likelihood profiling when non-normal distribution of the parameter distribution was observed.

Although the difference of the parameters between *Model 1* and *Model 3* was not so dramatic as that detected for *Model 2* (no apical side sampling), the $CL_{app,hep,u}$ (MPA) was over predict ~ 15% when *Model 3* was applied in gut-liver system. In addition, even considering the associated uncertainty of $CL_{app,hep,u}$ (MPA) from model 1, the value was less than the parameter estimated from *Model 3*. A clearer confirmation was provided by $CL_{app,hep,u}$ (MPA) in the simultaneous fitting (all), which reported a less parametric uncertainty compared to the gut-liver system. Therefore it was demonstrated that the sampling volume and the evaporation of the media played a not negligible role in the parametric estimation, as expected from the simulated profiles. From the simulations and fitting was clear that the simplification proposed was not acceptable and therefore it was rejected.

7. Impact of the gut cell volume and interconnection flow rate on clearance and distribution parameter estimation

7.1 Evaluation of the intestinal cells volume in the PK profiles

The low P_{app}(MPAG) compared to the MPA metabolic formation determined the compound sequestration in the intestinal cells (Figure S10). Therefore, the cells volume (V_e) is a relevant parameter as it affects recovery and parameter estimates. However it is not structurally identifiable thus, it needs to be fixed to the best known parameter values in order to get robust parametric estimation.

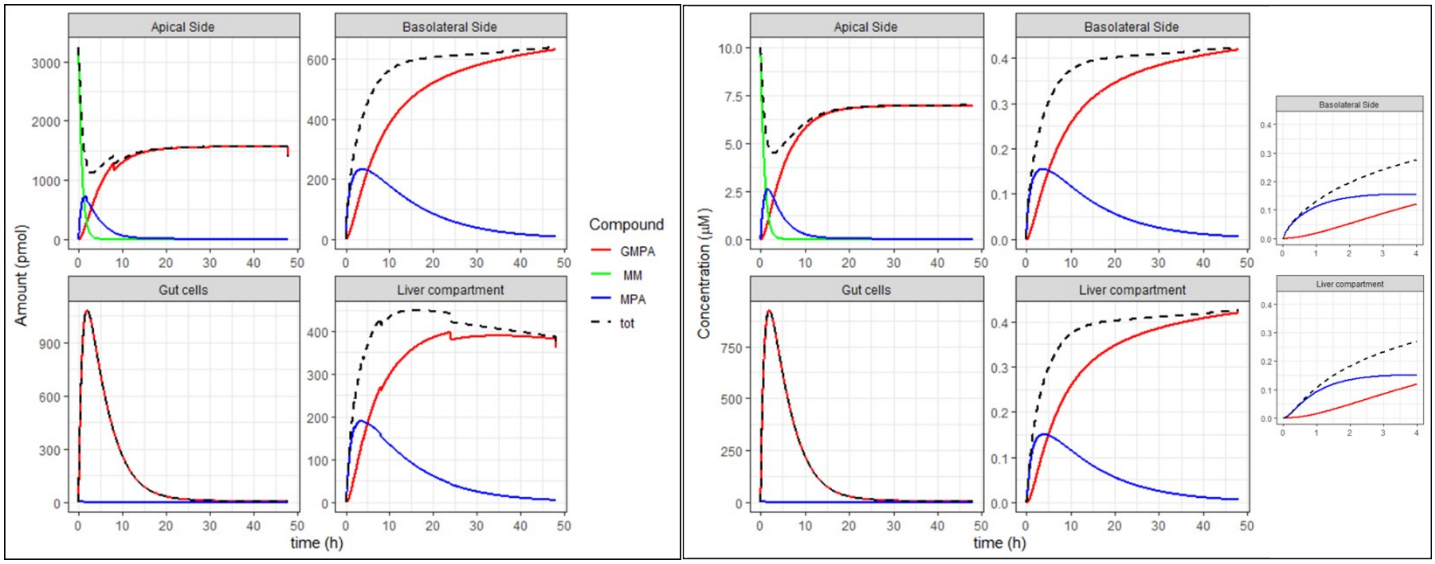

Figure S7.1. Representation of the total and compounds amount and concentration in all three compartments in addition to that in the intestinal cells compartment with an initial dose of mycophenolate mofetil of 10 μM in the apical side. Note: The concentration in in the basolateral side and in the liver compartment reached a homogenous concentration around 4 h of incubation. This feature was reported in the two small figures. However, a minimal concentration discrepancy between liver and basolateral compartment < 10% was already reached at 90 min.

Since the cells volume of the Caco2 and HT29 cells represented a critical parameter in the PK parametric estimation, firstly it was used as an estimated parameter in the model but it was demonstrated that it was not quantitatively identifiable. Therefore different volumes from literature were considered to be used as inputs.

1) Volume was extracted from literature data using Caco2 cells by florescent measurements and computational tools[1]. The author investigated the volume of the main compartments of the cells (nuclei, cytosol, and membrane-outer cytoplasm) in non-diving and diving cells. The total volume of non-diving cells (V_e) reported was 2.6 μL/10^6 cells [2].

2) In addition, the dimension of the HT29 cells was also investigated and its diameter was 16.6 µm. From an estimation of the cell volume assuming that on average the shape of the cells was perfectly spherical the volume was 2.4 µL/10^6 cells, which was very similar to that detected in the Caco2 cells (8% of volume discrepancy). Therefore, it was assumed that the volume of Caco2-HT29 cells in the experiment was not significantly different and equal to 2.6 µL/10^6 cells.

3) The data form the volume of enterocytes estimated by 25 donors was 1.7 µL/10^6 cells[3] and assuming a spherical shape of the cells. This value has been used as an example to show the impact of the cells volume in some circumstances.

It should be noted that the measure of the cell volume is not a trivial operation since depends on the experimental technique of cell culturing and the method of measuring the volume.

In order to evaluate the impact of the cell size the fitting of the gut-liver model was performed with both volumes from points 1 and 2. Although the data from point 1 and 2 are relatively in agreement, they might significantly influence the parametric estimation. The fitting outcome was applied and the results reported in Table S7. As expected, it was not observed any significant discrepancy on the PK estimation using Caco2 and HT29 cells volumes.

		Volume intestinal cells (V_e)		
Parameter		V_e = 2.6 (Caco2)	V_e = 2.4 (HT29)	V_e = 1.7 (enterocytes)
	Units	µL/10^6 cells		
$CL_{int,gut,u}$ (MM)	µL/min/10^6 cells	13	13	13
$CL_{int,gut,u}$ (MPA)	µL/min/10^6 cells	24	23	23
$CL_{app,hep,u}$ (MPA)	µL/min/10^6 cells	26	26	26
P_{app} (MPA)	nm/s	688	687	685
P_{app} (MPAG)	*nm/s*	*0.37 ± 0.07*	*0.34 ± 0.07*	*0.24 ± 0.06*
E_r (MPA)		3.7	3.7	3.7
E_r (MPAG)		2.9	2.9	2.9

Table S7.1. Evidence of the volume of the intestinal cells on the PK. The parameter uncertainty was reported for the affected parameter P_{app}(GMPA) reported in italic.

Although the enterocytes are epithelial cells as Caco2 and HT29, the different volume determine a significant difference in the P_{app}(GMPA). The highest discrepancy as expected was detected for P_{app}(MPAG), whereas the other parameters were negligibly influenced. It is interesting to see that the discrepancy of the P_{app}(MPAG) estimation reflected the difference on the V_e values between Caco2 and enterocytes volume. Indeed, the ratio of the V_e between Caco2 and enterocytes was ~1.5 which was approximatively the same of P_{app}(GMPA) estimated using both volumes. As expected the difference in volume of Caco2 cells and

HT29 was negligible (<10% for all parameters). Since the value of 2.6 µL/10^6 cells was generated by experimental evidence directly from Caco2 cells and the value was also in agreement with that evaluated in the HT29 cells it was used as input for the fitting and the parametric estimation.

7.2 Effect of gut-liver interconnection flow rate (Q_i)

The last evaluation regarded the impact of the interconnection flow rate in the parametric estimation. Therefore different fitting using the data from gut-liver system were applied in order to detect any substantial differences in the PK parameters using three different interconnection flow rate. The Q_i used in the experiments was 90 µL/min. However, the system had an uncertainty on the Qi of 20%, which determined a Q_i ranging from 72 to 108 µL/min. The three input values of Q_i which used in the fitting were generated based on the uncertainty provided by CN Bio Ltd. Therefore, the Q_i might generate a significant inter-well difference if the flow rate is not stable or the same in all wells and for the entire duration of the experiment. From Table S8 the PK parameters did not change significantly. It was demonstrated that with the range of expected Q_i the PK estimation was not significantly affected.

		Interconnection flow rate		
Parameter		Q_i =90	Q_i= 72	Q_i= 108
	Units	µL/min		
$CL_{int,gut,u}$ (MM)	µL/min/10^6 cells	13 ±1	12	13
$CL_{int,gut,u}$ (MPA)	µL/min/10^6 cells	24 ± 7	24	24
$CL_{app,hep,u}$ (MPA)	µL/min/10^6 cells	26 ± 3	26	26
P_{app} (MPA)	nm/s	688 ± 221	693	688
P_{app} (MPAG)	nm/s	0.37 ± 0.07	0.34	0.37
E_r (MPA)		3.7 ± 0.9	3.8	3.7
E_r (MPAG)		2.9 ± 0.6	2.9	2.9

Table S7.2. Impact of the Q_i in the parametric estimation.

8. Global Dynamic Sensitivity Analysis

Introduction

The robustness and uncertainty of a parameter estimates depend on multiple factors such as inter-well variability, error in the analytical method or procedure, but also on the selection of the sampling times. Optimized set of sampling points at the right compartment and time is crucial for an accurate and precise estimation. A complex system (e.g. PK parameters and compartments), required a large number of combinations for defining a set of sampling points. An optimization of the sampling times (Table 1) might be executed by global dynamic sensitivity analysis as reported in this work from a pilot experiment (data not shown). Combining gut and liver in a single system introduced uncertainty in some parameter estimates relative to the use of individual cell systems, namely $CL_{int,gut,u}$ (MPA), P_{app}(MPA), and E_r(MPA).

Method

In this work the method for the sensitivity analysis referred to that developed by Morris and available in R (*ODEsensitivity* library). In this the major output are μ_i*and σ_i. μ_i* is a measure for the overall influence of input x_i on the output (i.e., concentration-time profiles) and σ_i reflects the linearity of the influence[26]. A parameter with σ_i close to 0 suggests linear behavior whereas high value a nonlinear or interaction among the parameters. The analysis of each compartment in the gut-liver system was performed using the PK parameters with their uncertainty reported in Table 3 in the main manuscript and applying the features of *Model 1*.

Results

Most of the parameters i [$CL_{int,gut,u}$ (MM), $CL_{int,gut,u}$ (MPA), $CL_{app,hep,u}$ (MPA), P_{app}(MPA), P_{app}(MPAG), Er(MPA)] in the apical side showed the highest intensity (μ_i*) (Figure 8 and Figure S15 which reported σ associated to the respective μ_i*) in a short interval of time and majorly close to the start of the incubation (~ 5 h). In the basolateral and the liver compartments $CL_{app,hep,u}$ (MPA) and E_r (MPAG) had a highest μ_i* after 10 h and differently to the other parameters which showed high μ_i* at the first part of the incubation as in the apical side. From the pilot experiment, the experimental sampling times were opportunely selected in all compartments in order to cover early (mostly in the apical and basolateral compartment) and late sampling points (liver compartments) (Table 1). In order to further reduce the uncertainty and improve the robustness of $CL_{int,gut,u}$ (MPA), P_{app} (MPA), and E_r(MPA) the sensitivity analysis suggested to further intensify the sampling points at the first 4-5 h apical and basolateral-liver compartment, respectively.

Discussion

The suggestion of the sensitivity analysis to intensify the sampling points to improve the estimates of $CL_{int,gut,u}$ (MPA), P_{app} (MPA), and E_r(MPA), are experimentally difficult to implement. In the apical side the sampling volume of 25 µL reduced the total volume of more 25% and even though it was included into the fitting model, the removal of volume might drastically change the biological environment and the availability of nutrients present in the apical media. Therefore, the only plausible approach to increase the number of sampling times in the apical side may be the reduction of the sampling volume. Since the relatively high concentration of the compounds in the apical side it might be a reasonable strategy for mycophenolate mofetil investigation, but it cannot be generalized for every scenario. In the basolateral and liver compartment, an optimized number of samples were already performed in order to maintain a minimal work volume (between 2600 and 2250 µL) in accordance with the sampling and media evaporation (Figure S2). Contrarily to the apical side, in the liver compartment, the reduction of the sampling volume might not be easy to apply since the presence in the media of BSA which comports the use of the supernatant for the

preparation of the samples and therefore a higher volume is generally required. In addition, also the dilution factor between gut apical side and the basolateral and liver compartments of around 9 fold comports an additional challenge on the use of a reduced sampling volume due to sensitivity of the analytical method. With this evaluation, it was demonstrated the power of the global dynamic SA for a such complex system as the Gut-Liver OoC in order to get interesting information about the optimization of the sampling points. However, this approach needs to be considered as an explorative investigation and its outcomes need to be verified by experimental data as suggested even by the authors of the *ODEsensitivity* library.

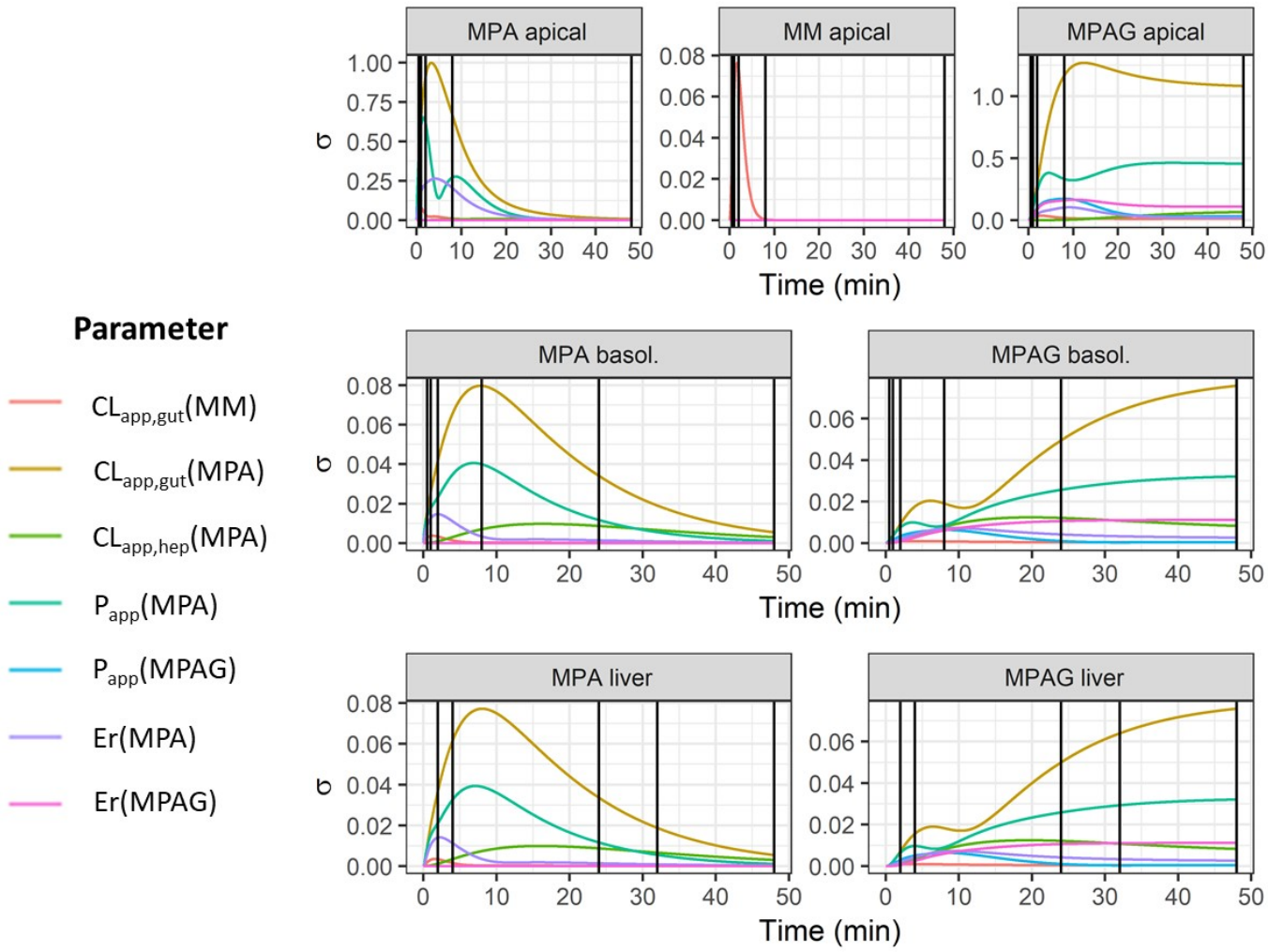

Figure S8.1. σ from global dynamic sensitivity analysis using the parametric uncertainty of the gut-liver system. The vertical lines in each graphs represented the sampling points (note that some of them in the apical and basolateral side are overlapped in the graph). The term"basol."means basolateral side in the gut compartment.

9. -2LL profiling of PK parameters

Introduction

The aim of this analysis is:

1) Verify the deterministic identifiability of the parameters

2) Explore the parametric uncertainty and its distribution

3) Provide an interval of uncertainty when the parameter uncertainty cannot be associated to a normal distribution [no standard deviation (SD)] in a confidence interval (CL) of 95%.

Method

This analysis was performed comparing the -2LL profiling for each parameter using no parametric constrain (all degrees of freedom) and a perturbation of the parameter from the unconstrained prediction. The log likelihood profiling with the Wilks test (log likelihood ratio test) was evaluated in all experimental systems and for the model applied for the simultaneous fitting. Various perturbations from -1 to 1 in the log domain were performed in addition to the unconstrained model. The analysis was performed in Phoenix using the *Profile* option under *Run Options* [2]-panel and applying Model1 towards gut-liver (Figure S11), gut-only (Figure S12), liver-only (Figure S13), and simultaneous fitting (Figure S14) conditions. The differences of − 2 log-likelihood between the evaluation over the unconstrained parametric prediction and that from imposing the constraint perturbation, follows a χ^2squared distribution. The 3.84, 2.71, and 1.00 represent the 95%, 90%, and 68% centile of the χ^2-squared distribution for 1 degree of freedom and they were reported in Figure S11-14.

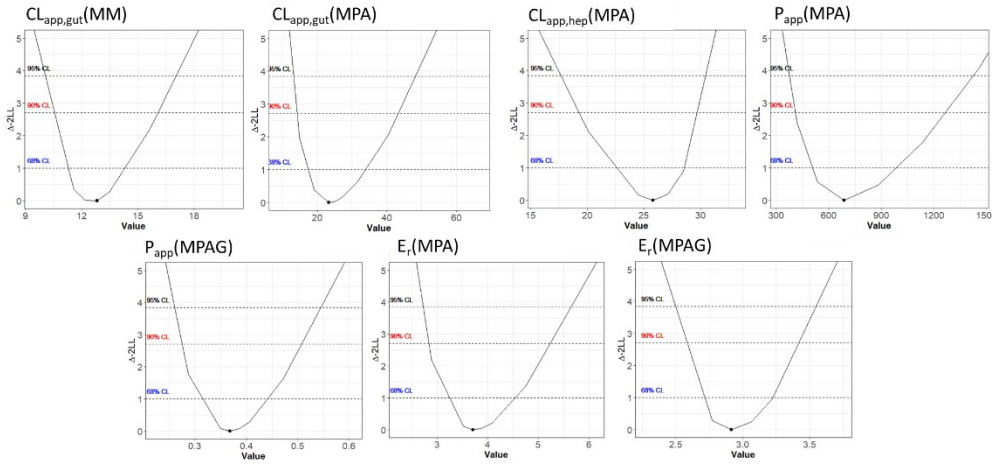

Figure S9.1. -2LL profiling in gut-liver system for all protein unbound estimated parameters. $P_{app,u}$(MPA), $CL_{int,gut,u}$(MPA), $CL_{app,hep,u}$(MPA), and E_r(MPA) were not considered to have a normal parametric distribution.

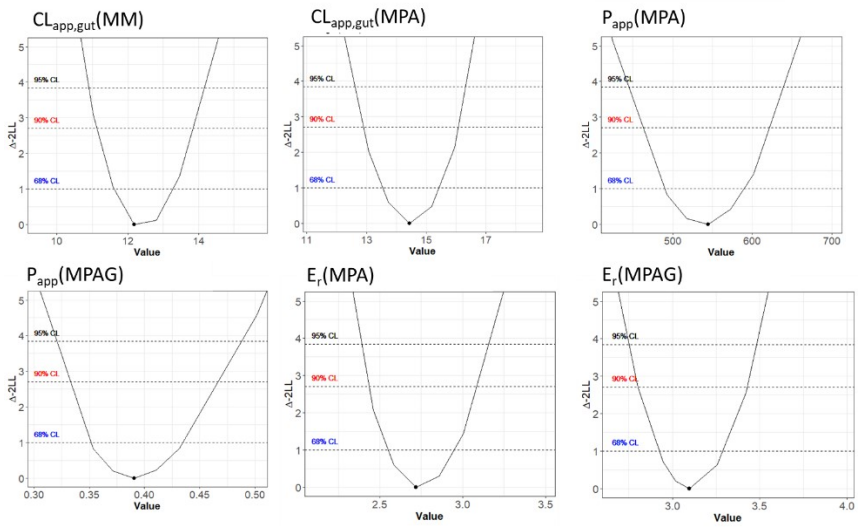

Figure S9.2. -2LL profiling in gut-only system for all estimated parameters

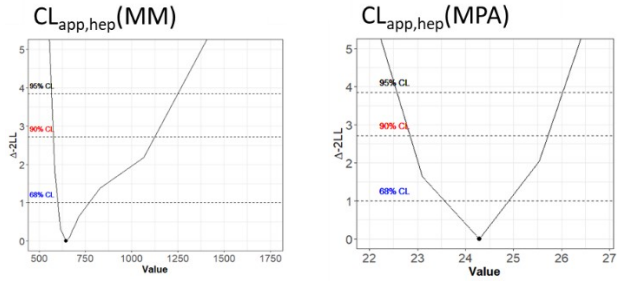

Figure S9.3. -2LL profiling in liver-only system for all estimated parameters

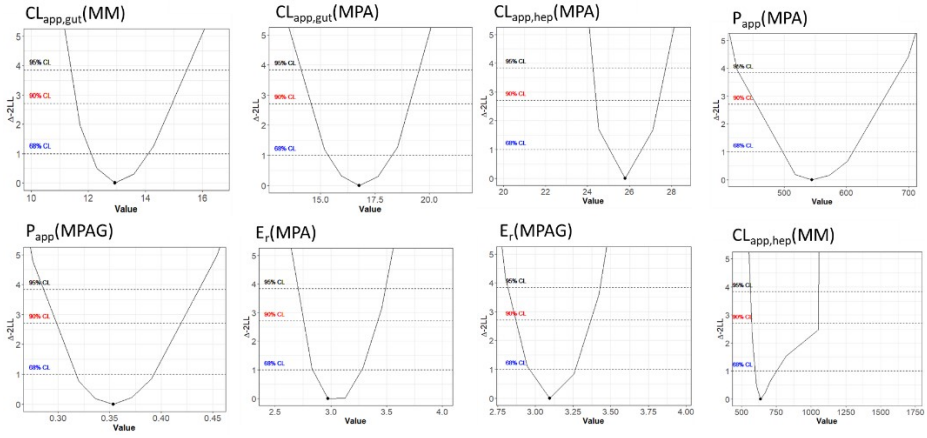

Figure S9.4. -2LL profiling in all simultaneous fitting condition for all estimated parameters. $CL_{app,hep,u}$(MM) and E_r(MPA) were not consider to have a normal parametric distribution.

Results and Discussion

From this analysis all parameters had a significant influence on the -2LL under all conditions demonstrating that the parameters were identifiable. However, it was also investigate the distribution of the parameters with a confidence level of 95%. A normal distribution of the parameters was observed in the gut-only system and all parameters were reported with the respective standard deviation (SD). In the gut-liver system the parameters $CL_{int,gut,u}$ (MPA), $CL_{app,hep,u}$(MPA), P_{app}(MPA), and E_r(MPA) showed a non-normal distribution and therefore the range with confidence level 95% were reported instead of the SD. In the liver-only and the simultaneous fitting $CL_{app,hep,u}$ (MM) showed a non-normal distribution and the uncertainty was reported as range of parameters. The explanation is due to the fact the only 3 points were available (including 0 min) since the fast depletion of the prodrug in the liver-only system. However, the estimated $CL_{app,hep,u}$ (MM) from liver-only and the simultaneous fitting were in accordance (discrepancy < 1%). This parameter is the less relevant for our investigation, since the prodrug is orally administered.

The procedure described above was used for the parametric estimation applied for the model verification reported in the previous sections in gut-liver system.

10. Graphical model representation and fitting profiles from *Model 1* of all three experimental systems and the simultaneous fitting.

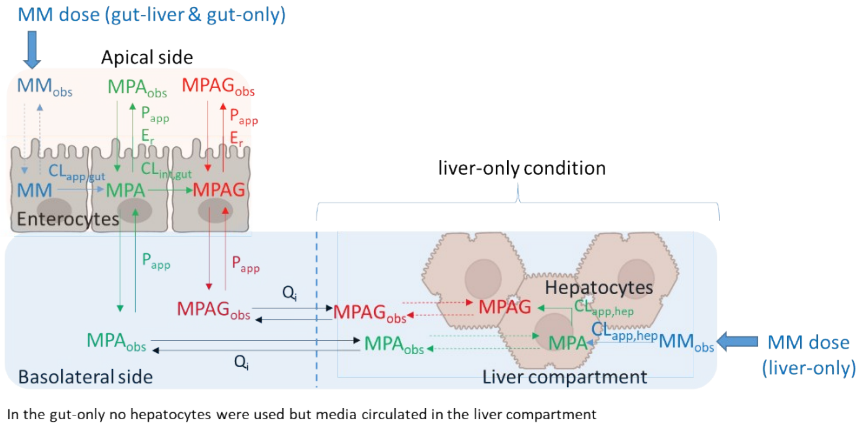

Figure S10.1. Schematic representation of the simultaneous fitting model where all the DMPK processes from the individual experiments were included.

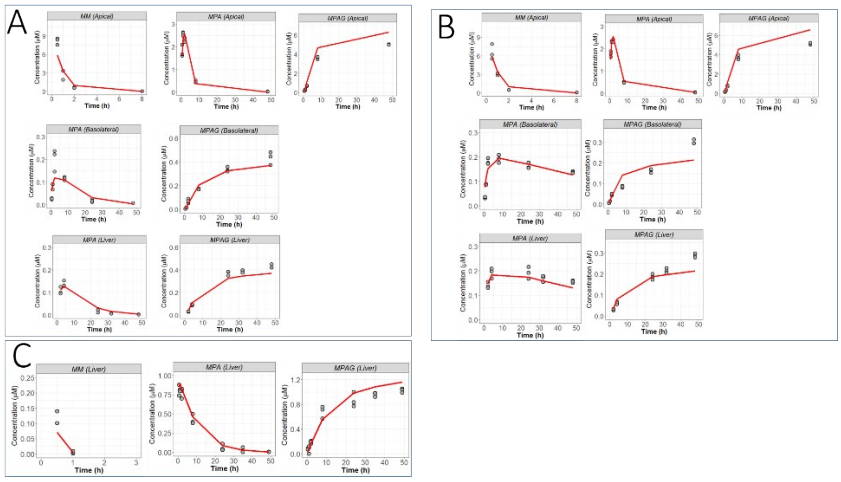

Figure S10.2. Goodness of fitting from gut-liver (A), gut-only (B) and liver-only (C) systems.

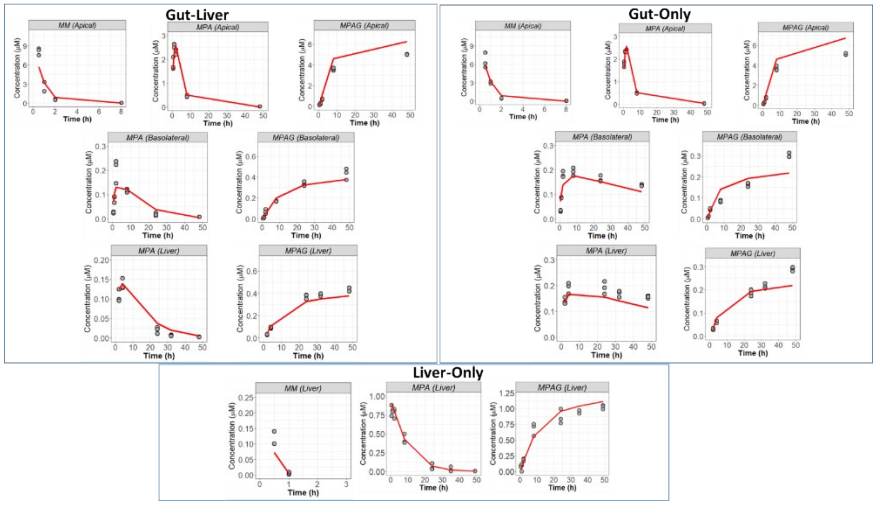

Figure S10.3. Goodness of fitting from gut-liver, gut-only and liver-only systems simultaneously fitted.

11.References

1. C. W. Tan, B. S. Gardiner, Y. Hirokawa, M. J. Layton, D. W. Smith and A. W. Burgess, *PloS one*, 2012, **7**, e31882.
2. M. Tahara, T. Inoue, Y. Miyakura, H. Horie, Y. Yasuda, H. Fujii, K. Kotake and K. Sugano, *Biochemical and Biophysical Research Communications*, 2013, **434**, 753-759.
3. M.-C. D. Ho, N. Ring, K. Amaral, U. Doshi and A. P. Li, *Drug metabolism and disposition*, 2017, **45**, 686-691.